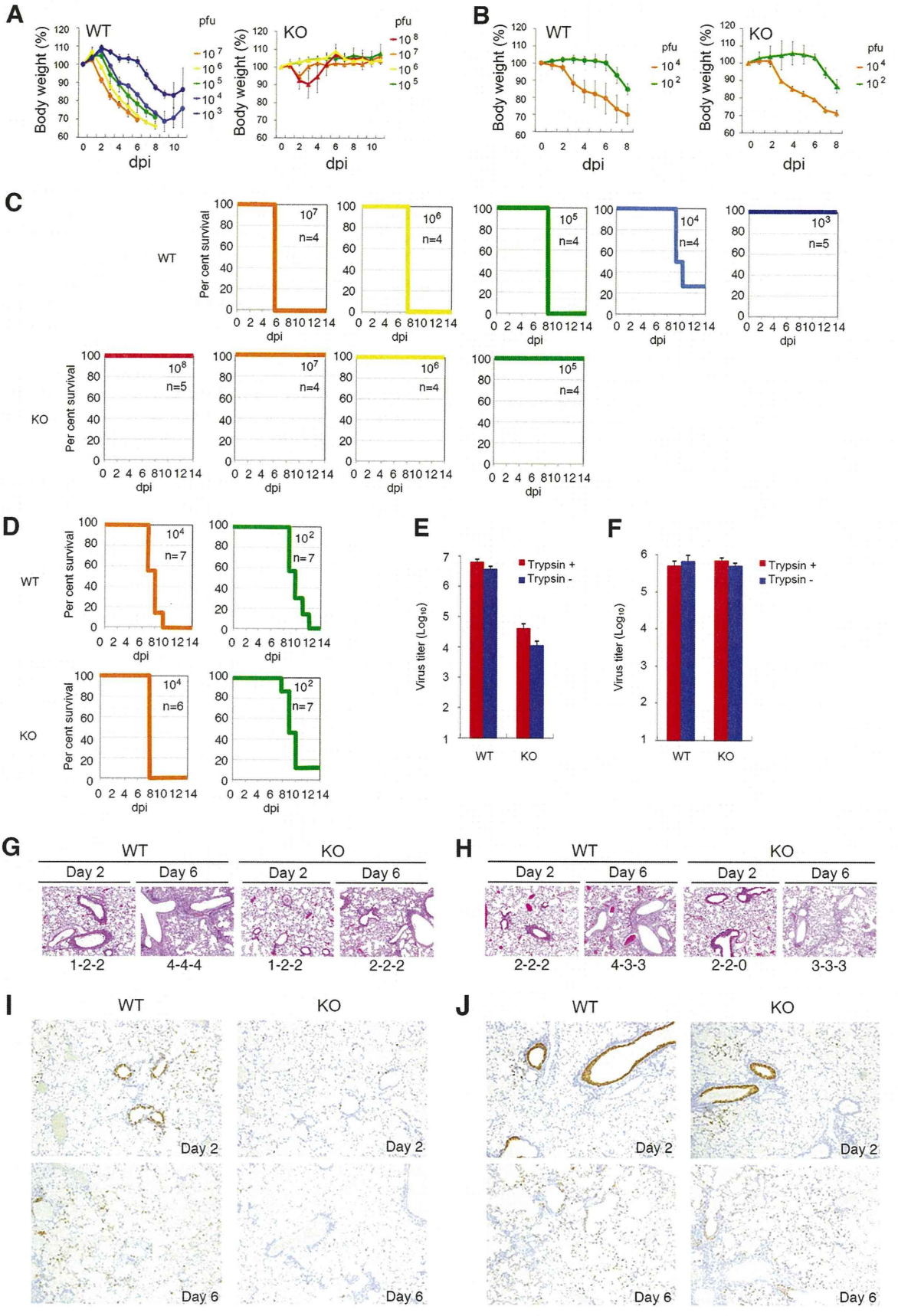
A
WT
KO
Body weight (%)
dpi
pfu
B
C
WT
KO
Per cent survival
n=4
n=5
D
n=7
n=6
E
Virus titer (Log10)
Trypsin +
Trypsin -
F
G
Day 2
Day 6
1-2-2
4-4-4
2-2-2
H
2-2-0
4-3-3
3-3-3
I
J

MAG mRNA isolation kit (Invitrogen). RNA strand-specific transcriptome sequencing (RNA-seq) libraries were prepared from ~50 ng of the purified poly(A) mRNA using a ScriptSeq v2 RNA-Seq Library Preparation kit (Epicentre). The prepared RNA-seq library was sequenced by using a GAIIx sequencer (Illumina). The obtained strand-specific short reads were analyzed by CLC Genome Workbench (v. 6.05) with mean expression normalization against *Mus musculus* reference genome sequences (GRCm38.p1), and genes showing significant differential expression were detected with a false discovery rate (FDR) of <0.05 and changes of $\geq$2-fold. The reads per kilobase of exon model per million mapped reads (RPKM) were estimated for each transcriptome experiment.

Titration of infectious units. To determine the infectious virus titers activated *in vivo*, monolayers of MDCK cells in 12-well plates were infected with serially diluted virus samples for 1 h at 4°C, washed twice with PBS, overlaid with DMEM–1% agarose, and incubated for 24 h at 37°C to allow the viruses to enter the cells. Trypsin was omitted to avoid HA cleavage before virus entry. At 24 h postinfection, the cell monolayers were additionally overlaid with DMEM–1% agarose supplemented with 2.0 μg/ml of trypsin to allow plaque formation. The virus titers obtained with this method were essentially equivalent to those obtained by immunofluorescence staining techniques (26), in which trypsin was omitted during the entire process of titration and individual infected cells, instead of plaques, were detected and counted. To determine the infectious titers of viruses that had not been activated *in vivo* but possessed infectious potential, virus samples were treated with 1.0 μg/ml of trypsin and subjected to a standard plaque assay.

Infection of mice. KO ($TMPRSS2^{-/-}$) and WT ($TMPRSS2^{+/+}$) C57BL/6 mice (6- to 7-week-old males or females) were challenged with MA-CA04[H1N1], MA-GZX[H3N2], VN1194[H5N1], or Anhui1 [H7N9]. For each mouse, 20 μl of virus solution containing different amounts of IAV was inoculated intranasally. For mock infection, the same volume of PBS was used. For each experimental group, 4 to 6 mice were used to monitor body weight. To analyze the *in vivo* activation and replication of IAV, WT and TMPRSS2 KO mice were challenged with 4.0×10^3 PFU of MA-CA04[H1N1] or 6.8×10^3 PFU of MA-GZX[H3N2]. Lung lavage fluids collected at 2, 4, and 6 days postinfection (dpi) and lung homogenates collected at 2 dpi were either untreated or treated with trypsin to determine the virus titers activated *in vivo* and *in vitro*, respectively. Three mice were used for each experimental group, and samples were collected separately from individual mice. For histopathological examinations, WT and TMPRSS2 KO mice were infected with 4.0×10^3 PFU (3.0×10^2 50% lethal doses [LD_{50}]) of MA-CA04[H1N1], 6.8×10^3 PFU (1.0×10^2 LD_{50}) of MA-GZX[H3N2], 1.0×10^4 PFU (1.0×10^2 LD_{50}) of VN1194[H5N1], or 4.0×10^6 PFU (1.0×10^2 LD_{50}) of Anhui1[H7N9]; euthanized; and autopsied at 2 and 6 dpi. Three mice were used for each experimental group.

Immunoblotting. The lung lavage fluids and lung homogenates were mixed with lysis buffer to make a final solution containing 150 mM NaCl, 50 mM Tris-HCl (pH 7.5), 4 mM EDTA, 0.1% sodium deoxycholate, 1% Nonidet P-40, and 0.1% SDS, containing a complete protease inhibitor mixture (Roche Diagnostics). The polypeptides were then separated by SDS-PAGE and immunoblotted. A rabbit antiserum raised against H3 (Sino Biological Inc.) was used for detection.

Nucleotide sequence accession number. The RNA-seq reads of the lung tissues from WT and TMPRSS2 KO mice are available at the DDBJ Sequence Read Archive under accession number DRA001103 (47,935,571 and 46,863,938 paired-end reads for WT and TMPRSS2 KO mice, respectively).

RESULTS

mTMPRSS2 proteolytically activates IAV HAs similarly to hTMPRSS2. To obtain a biological rationale for performing mouse experiments, we analyzed mTMPRSS2. Three-dimensional structural models of mTMPRSS2 and hTMPRSS2 showed strong conservation of amino acid residues near the protease active site (data not shown). Based on the strong homology between hTMPRSS2 and mTMPRSS2, these proteases were strongly suggested to have similar substrate specificities. However, the TMPRSS2 structures were strictly models, and biological analyses were performed. The analyses showed that all HAs of LP IAVs of the H1, H3, and H7 subtypes were cleaved by both mTMPRSS2 and hTMPRSS2 (Fig. 1A), and the cleaved HAs showed cell-cell fusion (syncytium formation) activity (Fig. 1B). As expected, cleavage and activation of HA of an HP IAV of the H5 subtype occurred independently of TMPRSS2 expression (Fig. 1A and B). Consistent with previous data (27), different molecular sizes of HA were detected in TMPRSS2-expressing cells, because the expression of TMPRSS2 modulates the HA glycosylation pattern (Fig. 1A).

TMPRSS2 is essential for the pathogenicity of H1N1 and H3N2 IAVs. TMPRSS2 KO mice, which possessed an ablating deletion including exons 3 to 13 of the TMPRSS2 gene, were generated in a complete C57BL/6 genetic background (Fig. 2). To confirm whether TMPRSS2 KO induced unexpected differential expression of other TTSPs, RNA-seq experiments were performed. The transcriptome analysis indicated that TMPRSS2 KO did not significantly affect the expressions of other TTSP genes and potential protease genes (Table 1). As an exception, the level of St14 appeared to be increased in the TMPRSS2 KO mouse lung (Table 1), but the raw count was still very low, and the change was judged to be insignificant based on the FDR analysis. However, our data did not exclude the possibility that the change was induced by TMPRSS2 gene KO. TMPRSS2 KO mice exhibited normal reproduction, development, and growth patterns, similarly to WT C57BL/6 mice, as observed for previously reported TMPRSS2 KO mice with a deletion of exons 10 to 13 in the TMPRSS2 gene (25).

Various doses of MA viruses of human LP IAV strains MA-CA04[H1N1] and MA-GZX[H3N2] were inoculated intranasally into WT and TMPRSS2 KO mice. All WT mice inoculated with $\geq 10^2$ PFU (7.5 LD_{50}) of MA-CA04[H1N1] died or required euthanasia (Fig. 3A and C). In strong contrast, TMPRSS2 KO mice challenged with up to 10^5 PFU (7.5×10^3 LD_{50}) showed neither clinical signs nor body weight loss (Fig. 3A and C). TMPRSS2 KO mice were also highly tolerant of lethal challenge infections with MA-

FIG 5 Role of TMPRSS2 in H5N1 and H7N9 IAV pathogenicity. (A and B) WT and TMPRSS2 KO mice were intranasally inoculated with different doses of Anhui1[H7N9] (A) or VN1194[H5N1] (B) ($n = 4$ to 6). The body weights were measured daily. Error bars represent standard deviations. (C and D) Survival curves of IAV-infected mice. WT and TMPRSS2 KO mice were challenged with different doses of Anhui1[H7N9] (C) or VN1194[H5N1] (D). For each experimental group, 4 to 7 mice were used. (E and F) WT and TMPRSS2 KO mice were intranasally inoculated with Anhui1[H7N9] ($n = 3$) or VN1194[H5N1] ($n = 3$). Lung homogenates at 4 dpi (D) were either untreated (Trypsin −) or treated with trypsin (Trypsin +) and used for virus titration. Error bars represent standard deviations. (G to J) Histopathological findings in the lungs of WT and TMPRSS2 KO mice infected with Anhui1[H7N9] (G and I) or VN1194[H5N1] (H and J). Data obtained by hematoxylin and eosin staining (magnification, ×10) (G and H) and immunohistochemistry for the IAV nucleocapsid protein (magnification, ×10) (I and J) are shown. The inflammation scores of individual mice ($n = 3$) are shown at the bottom of each panel (G and H): 0, no apparent changes; 1, minimal changes or bronchiolitis; 2, bronchiolitis and/or slight alveolitis; 3, mild alveolitis with neutrophils, monocytes/macrophages, or lymphocytes; 4, moderate alveolitis.

GZX[H3N2] (Fig. 3B and D). All TMPRSS2 KO mice infected with 10^5 PFU (1.5×10^3 LD_{50}) of MA-GZX[H3N2] showed moderate body weight loss but recovered completely (Fig. 3B and D).

Figure 3E to H shows the histopathology of lungs of mice infected with 4.0×10^3 PFU (3.0×10^2 LD_{50}) of MA-CA04[H1N1] or 6.8×10^3 PFU (1.0×10^2 LD_{50}) of MA-GZX[H3N2]. WT mice infected with each virus developed bronchiolitis and peribronchial inflammation, with a few foci of alveolitis at 2 dpi and mild to moderate alveolitis at 6 dpi (Fig. 3E and F). Viral antigens were detected in bronchial epithelial cells and alveolar lining cells in the lungs of WT mice at 2 dpi and had spread dramatically to the entire lungs by 6 dpi (Fig. 3G and H). In contrast, the lungs of KO mice infected with the same viruses exhibited significantly reduced levels of inflammation (Fig. 3E and F). Viral antigen-positive cells did not spread during the observation period (Fig. 3G and H). Viral antigens were almost completely eliminated from bronchiolar epithelial cells of KO mice by 6 dpi (Fig. 3G and H).

TMPRSS2 is essential for proteolytic activation of IAVs *in vivo*. To explore the cleavage of HA in the lungs, WT and TMPRSS2 KO mice were infected with 4.0×10^3 PFU (3.0×10^2 LD_{50}) of MA-CA04[H1N1] or 6.8×10^3 PFU (1.0×10^2 LD_{50}) of MA-GZX[H3N2]. At 6 dpi, lung lavage fluids were collected from mice infected with MA-GZX[H3N2] and analyzed for HA protein by SDS-PAGE and immunoblotting. Cleavage of HA was demonstrated in WT mice, as signals for the HA_1 and HA_2 subunits were clearly detected in these mice (Fig. 4A). In contrast, only the HA_0 precursor was detected in TMPRSS2 KO mice, and HA_1 and HA_2 remained undetectable (Fig. 4A). Similarly, lung homogenates of the infected mice were analyzed. HA was efficiently cleaved into HA_1 and HA_2 in the lung homogenates of WT mice (Fig. 4B). Meanwhile, the lung homogenates of TMPRSS2 KO mice showed HA_0 signals, but HA_1 and HA_2 were undetectable (Fig. 4B). These findings indicated that the HA protein of progeny viruses present in the respiratory tract had been cleaved in WT mice, while HA cleavage was severely impaired in TMPRSS2 KO mice. To verify whether the infectivity of the progeny viruses from each mouse lung was activated *in vivo*, lung lavage fluids at 2, 4, and 6 dpi and lung homogenates at 2 dpi were treated or untreated with trypsin *in vitro* and compared for infectivity *in vitro* to determine virus titers. At 2 dpi, the virus titers of MA-CA04[H1N1] and MA-GZX[H3N2] reached their peak levels in WT mice (Fig. 4C). The HAs of progeny viruses were shown to be fully activated in WT mice, since the virus infectivity titers without trypsin treatment (Fig. 4C and D) were similar to those after activation *in vitro* (Fig. 4C and D). The virus titers in the lungs of TMPRSS2 KO mice were much lower than those in the lungs of WT mice (Fig. 4C and D), showing restricted virus growth in TMPRSS2 KO mice. Importantly, the virus titers (Fig. 4C and D) were further increased 10 to 100 times after trypsin treatment *in vitro* (Fig. 4C and D). These data demonstrated that the great majority (90 to 99%) of the progeny virus particles failed to be proteolytically activated in TMPRSS2 KO mice.

TMPRSS2 is essential for LP H7N9 IAV, but dispensable for HP H5N1 IAV, to exhibit pathogenicity. The pathogenicity of a human isolate of an emerging LP H7N9 subtype virus, Anhui1 [H7N9], was also analyzed. Anhui1[H7N9] was inoculated intranasally into WT and TMPRSS2 KO mice. As shown in Fig. 5A and C, TMPRSS2 KO mice were highly tolerant of H7N9 virus infection. All WT mice infected with 10^5 PFU (5.0×10 LD_{50}) of Anhui1[H7N9] died or required euthanasia by 8 dpi (Fig. 5A and C). In contrast, all TMPRSS2 KO mice infected with the same dose (10^5 PFU [5.0×10 LD_{50}]) showed no clinical signs, and those infected with a 1,000-times-higher dose, 10^8 PFU (5.0×10^4 LD_{50}), showed only temporary and mild body weight loss (Fig. 5A). The virus titers in the KO mouse lungs were much lower than those in the WT mouse lungs (Fig. 5E). Histopathological examinations of mouse lungs infected with 4.0×10^6 PFU of Anhui1[H7N9] showed that Anhui1[H7N9] spread poorly in the lungs of TMPRSS2 KO mice (Fig. 5G and I).

In contrast to the findings for the LP IAVs described above, a human isolate of an HP H5N1 subtype virus, VN1194[H5N1], caused severe body weight loss, neurological symptoms, and death or requirement for euthanasia by 8 or 9 dpi in both WT and TMPRSS2 KO mice infected with 10^4 PFU (2.0×10^3 LD_{50}) of VN1194[H5N1] (Fig. 5B and D). The survival curves of WT and TMPRSS2 KO mice infected with 10^2 PFU (5.0×10 LD_{50}) of VN1194[H5N1] were also similar to one another (Fig. 5B and D). The virus titers in the lungs were equivalent between WT and KO mice (Fig. 5F). Histopathological examinations of mouse lungs infected with 1.0×10^4 PFU of VN1194[H5N1] demonstrated that VN1194[H5N1] spread efficiently in a similar manner in the lungs of WT and TMPRSS2 KO mice (Fig. 5H and J). The overall results indicated that, unlike LP IAVs, proteolytic activation of the HP H5N1 virus occurred in mouse lungs independently of TMPRSS2.

DISCUSSION

In the last decade, we have experienced outbreaks of a swine-origin LP H1N1 IAV and the severe acute respiratory syndrome (SARS) coronavirus (28, 29). These outbreaks proved that respiratory viruses can currently spread rapidly and that the available strategies are insufficiently effective to prevent global transmission of emerging respiratory viruses (28). At this time, H5N1 and H7N9 IAVs and the Middle East respiratory syndrome (MERS) coronavirus are potential threats for humans (29, 30).

The present study has provided concrete evidence that TMPRSS2 expression is essential for *in vivo* replication of emerging H7N9 and seasonal IAVs and that this protease primarily determines IAV pathogenicity. Based on the strong homology between hTMPRSS2 and mTMPRSS2, hTMPRSS2 is strongly suggested to play a similar role in the activation and pathogenicity of human IAVs *in vivo*. In human airway bronchial epithelial cells, TMPRSS2 is expressed by type 1 and type 2 pneumocytes of the alveolar epithelium and alveolar macrophages (12, 31). In the airway, IAV particles are released exclusively from the apical membrane (32). To achieve this, the IAV HA protein is specifically targeted to the apical plasma membrane (33, 34), and TMPRSS2 is selectively expressed at the apical membrane of airway epithelial cells (35). Taking these data into consideration, it is most likely that LP IAVs use primarily the specific host protease TMPRSS2 for HA activation in the lungs. However, our data do not exclude the possibility that TMPRSS2 may activate a precursor of another protease(s) that finally induces HA activation. Nevertheless, our data showing the critical role of TMPRSS2 expressed in the respiratory tract in the activation of IAV pathogenicity *in vivo* support the concept of host protease-mediated pathogenicity of IAVs (7–9).

The present findings suggest that TMPRSS2 is a good target for the development of anti-LP IAV drugs. The membrane-anchoring and cytoplasmic domains of TTSPs regulate cellular trafficking

and localization of TTSPs, thereby enabling temporal and spatial regulation of substrate processing (36–38). Accordingly, by targeting specific substrates such as peptide hormones, growth factors, differentiation factors, receptors, and adhesion molecules, TTSPs play a variety of critical roles in developmental stages and physiological events (36–38). A previous study suggested that TMPRSS2 regulates Na^+ currents (39). However, the physiological roles of TMPRSS2 remain to be elucidated (40), because TMPRSS2 KO mice showed a normal phenotype.

During the submission process for the present paper, Hatesuer et al. (41) reported a similar study demonstrating a critical role of TMPRSS2 in the pathogenicity of H1N1 and H3N2 IAVs in mice. They used a previously reported TMPRSS2 KO mouse strain with a deletion of exons 10 to 13 in the TMPRSS2 gene (25, 41). The TMPRSS2 KO mice with a deletion of exons 3 to 13 in the TMPRSS2 gene established in the present study exhibited phenotypes very similar to those of their mice, providing a very strong conclusion that TMPRSS2 expression is essential for IAV pathogenesis. Interestingly, in agreement with their data (41), our study demonstrated that replication of H1N1 IAV was more severely restricted in TMPRSS2 KO mice than that of H3N2 IAV. Therefore, cleavage of the H1 subtype appears to be more strongly dependent on TMPRSS2 expression than cleavage of the H3 subtype.

Finally, TTSPs have a clear substrate specificity (37). Nevertheless, various respiratory viruses, including the SARS coronavirus (12, 42–44), MERS coronavirus (14), human metapneumovirus (11), and parainfluenza viruses (13), also use TMPRSS2 for their activation. These observations imply that a variety of respiratory viruses may specifically exploit TMPRSS2 for activation. Drugs that inhibit TMPRSS2 are therefore expected to be effective against a wide spectrum of respiratory viruses. Meanwhile, different types of drugs targeting ubiquitous proteases other than TMPRSS2 may be required for HP IAVs such as the H5N1 virus subtype.

ACKNOWLEDGMENTS

The ES cells used for this research project were generated by the Trans-NIH Knockout Mouse Project (KOMP) and obtained from the KOMP Repository (http://www.komp.org/). NIH grants to VelociGene at Regeneron Inc. (U01HG004085) and the CSD Consortium (U01HG004080) funded the generation of gene-targeted ES cells for 8,500 genes in the KOMP Program, which were archived and distributed by the KOMP Repository at UC Davis and CHORI (U42RR024244). This work was supported by grants-in-aid from the Ministry of Education, Science, Sports and Culture of Japan (KAKENHI; 23390114), the Takeda Science Foundation, and ERATO, Japan, and by a National Institute of Allergy and Infectious Diseases Public Health Service research grant.

We thank Yuelong Shu, Chinese Center for Disease Control and Prevention, and Le Quynh Mai, National Institute of Hygiene and Epidemiology, for providing H7N9 IAV and H5N1 IAV, respectively; R. A. Lamb, Northwestern University, for providing anti-IAV serum; and E. Takashita, M. Shirakura, H. Asanuma, H. Fukuhara, A. Sato, N. Nagata, Y. Sato, and all our members in the Department of Virology 3, NIID, for suggestions and technical support.

REFERENCES

1. Kido H, Okumura Y, Takahashi E, Pan HY, Wang S, Yao D, Yao M, Chida J, Yano M. 2012. Role of host cellular proteases in the pathogenesis of influenza and influenza-induced multiple organ failure. Biochim. Biophys. Acta 1824:186–194. http://dx.doi.org/10.1016/j.bbapap.2011.07.001.
2. Bottcher-Friebertshauser E, Klenk HD, Garten W. 2013. Activation of influenza viruses by proteases from host cells and bacteria in the human airway epithelium. Pathog. Dis. 69:87–100. http://dx.doi.org/10.1111/2049-632X.12053.
3. Beaulieu A, Gravel E, Cloutier A, Marois I, Colombo E, Desilets A, Verreault C, Leduc R, Marsault E, Richter MV. 2013. Matriptase proteolytically activates influenza virus and promotes multicycle replication in the human airway epithelium. J. Virol. 87:4237–4251. http://dx.doi.org/10.1128/JVI.03005-12.
4. Baron J, Tarnow C, Mayoli-Nussle D, Schilling E, Meyer D, Hammami M, Schwalm F, Steinmetzer T, Guan Y, Garten W, Klenk HD, Bottcher-Friebertshauser E. 2013. Matriptase, HAT, and TMPRSS2 activate the hemagglutinin of H9N2 influenza A viruses. J. Virol. 87:1811–1820. http://dx.doi.org/10.1128/JVI.02320-12.
5. Galloway SE, Reed ML, Russell CJ, Steinhauer DA. 2013. Influenza HA subtypes demonstrate divergent phenotypes for cleavage activation and pH of fusion: implications for host range and adaptation. PLoS Pathog. 9:e1003151. http://dx.doi.org/10.1371/journal.ppat.1003151.
6. Hamilton BS, Gludish DW, Whittaker GR. 2012. Cleavage activation of the human-adapted influenza virus subtypes by matriptase reveals both subtype and strain specificities. J. Virol. 86:10579–10586. http://dx.doi.org/10.1128/JVI.00306-12.
7. Bosch FX, Garten W, Klenk HD, Rott R. 1981. Proteolytic cleavage of influenza virus hemagglutinins: primary structure of the connecting peptide between HA1 and HA2 determines proteolytic cleavability and pathogenicity of avian influenza viruses. Virology 113:725–735. http://dx.doi.org/10.1016/0042-6822(81)90201-4.
8. Kawaoka Y, Webster RG. 1988. Sequence requirements for cleavage activation of influenza virus hemagglutinin expressed in mammalian cells. Proc. Natl. Acad. Sci. U. S. A. 85:324–328. http://dx.doi.org/10.1073/pnas.85.2.324.
9. Rott R, Klenk HD, Nagai Y, Tashiro M. 1995. Influenza viruses, cell enzymes, and pathogenicity. Am. J. Respir. Crit. Care Med. 152:S16–S19. http://dx.doi.org/10.1164/ajrccm/152.4_Pt_2.S16.
10. Bottcher E, Matrosovich T, Beyerle M, Klenk HD, Garten W, Matrosovich M. 2006. Proteolytic activation of influenza viruses by serine proteases TMPRSS2 and HAT from human airway epithelium. J. Virol. 80:9896–9898. http://dx.doi.org/10.1128/JVI.01118-06.
11. Shirogane Y, Takeda M, Iwasaki M, Ishiguro N, Takeuchi H, Nakatsu Y, Tahara M, Kikuta H, Yanagi Y. 2008. Efficient multiplication of human metapneumovirus in Vero cells expressing the transmembrane serine protease TMPRSS2. J. Virol. 82:8942–8946. http://dx.doi.org/10.1128/JVI.00676-08.
12. Matsuyama S, Nagata N, Shirato K, Kawase M, Takeda M, Taguchi F. 2010. Efficient activation of the severe acute respiratory syndrome coronavirus spike protein by the transmembrane protease TMPRSS2. J. Virol. 84:12658–12664. http://dx.doi.org/10.1128/JVI.01542-10.
13. Abe M, Tahara M, Sakai K, Yamaguchi H, Kanou K, Shirato K, Kawase M, Noda M, Kimura H, Matsuyama S, Fukuhara H, Mizuta K, Maenaka K, Ami Y, Esumi M, Kato A, Takeda M. 2013. TMPRSS2 is an activating protease for respiratory parainfluenza viruses. J. Virol. 87:11930–11935. http://dx.doi.org/10.1128/JVI.01490-13.
14. Shirato K, Kawase M, Matsuyama S. 2013. Middle East respiratory syndrome coronavirus (MERS-CoV) infection mediated by the transmembrane serine protease TMPRSS2. J. Virol. 87:12552–12561. http://dx.doi.org/10.1128/JVI.01890-13.
15. Gierer S, Bertram S, Kaup F, Wrensch F, Heurich A, Kramer-Kuhl A, Welsch K, Winkler M, Meyer B, Drosten C, Dittmer U, von Hahn T, Simmons G, Hofmann H, Pohlmann S. 2013. The spike protein of the emerging betacoronavirus EMC uses a novel coronavirus receptor for entry, can be activated by TMPRSS2, and is targeted by neutralizing antibodies. J. Virol. 87:5502–5511. http://dx.doi.org/10.1128/JVI.00128-13.
16. Bertram S, Dijkman R, Habjan M, Heurich A, Gierer S, Glowacka I, Welsch K, Winkler M, Schneider H, Hofmann-Winkler H, Thiel V, Pohlmann S. 2013. TMPRSS2 activates the human coronavirus 229E for cathepsin-independent host cell entry and is expressed in viral target cells in the respiratory epithelium. J. Virol. 87:6150–6160. http://dx.doi.org/10.1128/JVI.03372-12.
17. Sakabe S, Ozawa M, Takano R, Iwastuki-Horimoto K, Kawaoka Y. 2011. Mutations in PA, NP, and HA of a pandemic (H1N1) 2009 influenza virus contribute to its adaptation to mice. Virus Res. 158:124–129. http://dx.doi.org/10.1016/j.virusres.2011.03.022.
18. Yoshikawa T, Matsuo K, Matsuo K, Suzuki Y, Nomoto A, Tamura S, Kurata T, Sata T. 2004. Total viral genome copies and virus-Ig complexes

after infection with influenza virus in the nasal secretions of immunized mice. J. Gen. Virol. 85:2339–2346. http://dx.doi.org/10.1099/vir.0.79892-0.
19. Gao P, Watanabe S, Ito T, Goto H, Wells K, McGregor M, Cooley AJ, Kawaoka Y. 1999. Biological heterogeneity, including systemic replication in mice, of H5N1 influenza A virus isolates from humans in Hong Kong. J. Virol. 73:3184–3189.
20. Watanabe T, Kiso M, Fukuyama S, Nakajima N, Imai M, Yamada S, Murakami S, Yamayoshi S, Iwatsuki-Horimoto K, Sakoda Y, Takashita E, McBride R, Noda T, Hatta M, Imai H, Zhao D, Kishida N, Shirakura M, de Vries RP, Shichinohe S, Okamatsu M, Tamura T, Tomita Y, Fujimoto N, Goto K, Katsura H, Kawakami E, Ishikawa I, Watanabe S, Ito M, Sakai-Tagawa Y, Sugita Y, Uraki R, Yamaji R, Eisfeld AJ, Zhong G, Fan S, Ping J, Maher EA, Hanson A, Uchida Y, Saito T, Ozawa M, Neumann G, Kida H, Odagiri T, Paulson JC, Hasegawa H, Tashiro M, Kawaoka Y. 2013. Characterization of H7N9 influenza A viruses isolated from humans. Nature 501:551–555. http://dx.doi.org/10.1038/nature12392.
21. Roy A, Kucukural A, Zhang Y. 2010. I-TASSER: a unified platform for automated protein structure and function prediction. Nat. Protoc. 5:725–738. http://dx.doi.org/10.1038/nprot.2010.5.
22. Guex N, Peitsch MC. 1997. SWISS-MODEL and the Swiss-PdbViewer: an environment for comparative protein modeling. Electrophoresis 18:2714–2723. http://dx.doi.org/10.1002/elps.1150181505.
23. Laskowski RA, MacArthur MW, Moss DS, Thornton MJ. 1993. PROCHECK: a program to check the stereochemistry of protein structures. J. Appl. Crystallogr. 26:283–291. http://dx.doi.org/10.1107/S0021889892009944.
24. Eisenberg D, Luthy R, Bowie JU. 1997. VERIFY3D: assessment of protein models with three-dimensional profiles. Methods Enzymol. 277:396–404. http://dx.doi.org/10.1016/S0076-6879(97)77022-8.
25. Kim TS, Heinlein C, Hackman RC, Nelson PS. 2006. Phenotypic analysis of mice lacking the Tmprss2-encoded protease. Mol. Cell. Biol. 26:965–975. http://dx.doi.org/10.1128/MCB.26.3.965-975.2006.
26. Tashiro M, Ciborowski P, Klenk HD, Pulverer G, Rott R. 1987. Role of Staphylococcus protease in the development of influenza pneumonia. Nature 325:536–537. http://dx.doi.org/10.1038/325536a0.
27. Bertram S, Glowacka I, Blazejewska P, Soilleux E, Allen P, Danisch S, Steffen I, Choi SY, Park Y, Schneider H, Schughart K, Pohlmann S. 2010. TMPRSS2 and TMPRSS4 facilitate trypsin-independent spread of influenza virus in Caco-2 cells. J. Virol. 84:10016–10025. http://dx.doi.org/10.1128/JVI.00239-10.
28. Waterer G. 2011. Controlling epidemic viral infection. Curr. Opin. Infect. Dis. 24:130–136. http://dx.doi.org/10.1097/QCO.0b013e328343b720.
29. Graham RL, Donaldson EF, Baric RS. 2013. A decade after SARS: strategies for controlling emerging coronaviruses. Nat. Rev. Microbiol. 11:836–848. http://dx.doi.org/10.1038/nrmicro3143.
30. Cowling BJ, Jin L, Lau EH, Liao Q, Wu P, Jiang H, Tsang TK, Zheng J, Fang VJ, Chang Z, Ni MY, Zhang Q, Ip DK, Yu J, Li Y, Wang L, Tu W, Meng L, Wu JT, Luo H, Li Q, Shu Y, Li Z, Feng Z, Yang W, Wang Y, Leung GM, Yu H. 2013. Comparative epidemiology of human infections with avian influenza A H7N9 and H5N1 viruses in China: a population-based study of laboratory-confirmed cases. Lancet 382:129–137. http://dx.doi.org/10.1016/S0140-6736(13)61171-X.
31. Bertram S, Heurich A, Lavender H, Gierer S, Danisch S, Perin P, Lucas JM, Nelson PS, Pohlmann S, Soilleux EJ. 2012. Influenza and SARS-coronavirus activating proteases TMPRSS2 and HAT are expressed at multiple sites in human respiratory and gastrointestinal tracts. PLoS One 7:e35876. http://dx.doi.org/10.1371/journal.pone.0035876.
32. Rodriguez Boulan E, Sabatini DD. 1978. Asymmetric budding of viruses in epithelial monlayers [*sic*]: a model system for study of epithelial polarity. Proc. Natl. Acad. Sci. U. S. A. 75:5071–5075. http://dx.doi.org/10.1073/pnas.75.10.5071.
33. Nayak DP, Barman S. 2002. Role of lipid rafts in virus assembly and budding. Adv. Virus Res. 58:1–28. http://dx.doi.org/10.1016/S0065-3527(02)58001-5.
34. Takeda M, Leser GP, Russell CJ, Lamb RA. 2003. Influenza virus hemagglutinin concentrates in lipid raft microdomains for efficient viral fusion. Proc. Natl. Acad. Sci. U. S. A. 100:14610–14617. http://dx.doi.org/10.1073/pnas.2235620100.
35. Jacquinet E, Rao NV, Rao GV, Hoidal JR. 2000. Cloning, genomic organization, chromosomal assignment and expression of a novel mosaic serine proteinase: epitheliasin. FEBS Lett. 468:93–100. http://dx.doi.org/10.1016/S0014-5793(00)01196-0.
36. Hooper JD, Clements JA, Quigley JP, Antalis TM. 2001. Type II transmembrane serine proteases. Insights into an emerging class of cell surface proteolytic enzymes. J. Biol. Chem. 276:857–860. http://dx.doi.org/10.1074/jbc.R000020200.
37. Antalis TM, Buzza MS, Hodge KM, Hooper JD, Netzel-Arnett S. 2010. The cutting edge: membrane-anchored serine protease activities in the pericellular microenvironment. Biochem. J. 428:325–346. http://dx.doi.org/10.1042/BJ20100046.
38. Bugge TH, Antalis TM, Wu Q. 2009. Type II transmembrane serine proteases. J. Biol. Chem. 284:23177–23181. http://dx.doi.org/10.1074/jbc.R109.021006.
39. Donaldson SH, Hirsh A, Li DC, Holloway G, Chao J, Boucher RC, Gabriel SE. 2002. Regulation of the epithelial sodium channel by serine proteases in human airways. J. Biol. Chem. 277:8338–8345. http://dx.doi.org/10.1074/jbc.M105044200.
40. Antalis TM, Bugge TH, Wu Q. 2011. Membrane-anchored serine proteases in health and disease. Prog. Mol. Biol. Transl. Sci. 99:1–50. http://dx.doi.org/10.1016/B978-0-12-385504-6.00001-4.
41. Hatesuer B, Bertram S, Mehnert N, Bahgat MM, Nelson PS, Pöhlman S, Schughart K. 2013. Tmprss2 is essential for influenza H1N1 virus pathogenesis in mice. PLoS Pathog. 9:e1003774. http://dx.doi.org/10.1371/journal.ppat.1003774.
42. Shulla A, Heald-Sargent T, Subramanya G, Zhao J, Perlman S, Gallagher T. 2011. A transmembrane serine protease is linked to the severe acute respiratory syndrome coronavirus receptor and activates virus entry. J. Virol. 85:873–882. http://dx.doi.org/10.1128/JVI.02062-10.
43. Glowacka I, Bertram S, Muller MA, Allen P, Soilleux E, Pfefferle S, Steffen I, Tsegaye TS, He Y, Gnirss K, Niemeyer D, Schneider H, Drosten C, Pohlmann S. 2011. Evidence that TMPRSS2 activates the severe acute respiratory syndrome coronavirus spike protein for membrane fusion and reduces viral control by the humoral immune response. J. Virol. 85:4122–4134. http://dx.doi.org/10.1128/JVI.02232-10.
44. Bertram S, Glowacka I, Muller MA, Lavender H, Gnirss K, Nehlmeier I, Niemeyer D, He Y, Simmons G, Drosten C, Soilleux EJ, Jahn O, Steffen I, Pohlmann S. 2011. Cleavage and activation of the severe acute respiratory syndrome coronavirus spike protein by human airway trypsin-like protease. J. Virol. 85:13363–13372. http://dx.doi.org/10.1128/JVI.05300-11.

Journal of Virology

Influenza A Virus Hemagglutinin and Neuraminidase Mutually Accelerate Their Apical Targeting through Clustering of Lipid Rafts

Takashi Ohkura, Fumitaka Momose, Reiko Ichikawa, Kaoru Takeuchi and Yuko Morikawa

J. Virol. **2014, 88(17):10039. DOI: 10.1128/JVI.00586-14.**
Published Ahead of Print 25 June 2014.

JVI
Journals.ASM.org

Influenza A Virus Hemagglutinin and Neuraminidase Mutually Accelerate Their Apical Targeting through Clustering of Lipid Rafts

Takashi Ohkura,[a] Fumitaka Momose,[a] Reiko Ichikawa,[a] Kaoru Takeuchi,[b] Yuko Morikawa[a]

Kitasato Institute for Life Sciences and Graduate School of Infection Control Sciences, Kitasato University, Tokyo, Japan[a]; Department of Environmental Microbiology, Division of Biomedical Science, Faculty of Medicine, University of Tsukuba, Tsukuba, Ibaraki, Japan[b]

ABSTRACT

In polarized epithelial cells, influenza A virus hemagglutinin (HA) and neuraminidase (NA) are intrinsically associated with lipid rafts and target the apical plasma membrane for viral assembly and budding. Previous studies have indicated that the transmembrane domain (TMD) and cytoplasmic tail (CT) of HA and NA are required for association with lipid rafts, but the raft dependencies of their apical targeting are controversial. Here, we show that coexpression of HA with NA accelerated their apical targeting through accumulation in lipid rafts. HA was targeted to the apical plasma membrane even when expressed alone, but the kinetics was much slower than that of HA in infected cells. Coexpression experiments revealed that apical targeting of HA and NA was accelerated by their coexpression. The apical targeting of HA was also accelerated by coexpression with M1 but not M2. The mutations in the outer leaflet of the TMD and the deletion of the CT in HA and NA that reduced their association with lipid rafts abolished the acceleration of their apical transport, indicating that the lipid raft association is essential for efficient apical trafficking of HA and NA. An *in situ* proximity ligation assay (PLA) revealed that HA and NA were accumulated and clustered in the cytoplasmic compartments only when both were associated with lipid rafts. Analysis with mutant viruses containing nonraft HA/NA confirmed these findings. We further analyzed lipid raft markers by *in situ* PLA and suggest a possible mechanism of the accelerated apical transport of HA and NA via clustering of lipid rafts.

IMPORTANCE

Lipid rafts serve as sites for viral entry, particle assembly, and budding, leading to efficient viral replication. The influenza A virus utilizes lipid rafts for apical plasma membrane targeting and particle budding. The hemagglutinin (HA) and neuraminidase (NA) of influenza virus, key players for particle assembly, contain determinants for apical sorting and lipid raft association. However, it remains to be elucidated how lipid rafts contribute to the apical trafficking and budding. We investigated the relation of lipid raft association of HA and NA to the efficiency of apical trafficking. We show that coexpression of HA and NA induces their accumulation in lipid rafts and accelerates their apical targeting, and we suggest that the accelerated apical transport likely occurs by clustering of lipid rafts at the TGN. This finding provides the first evidence that two different raft-associated viral proteins induce lipid raft clustering, thereby accelerating apical trafficking of the viral proteins.

Influenza virus is an enveloped, negative-stranded, segmented RNA virus belonging to the *Orthomyxoviridae* family. The virion consists of three integral membrane proteins, hemagglutinin (HA), neuraminidase (NA), and ion channel protein M2. A layer of matrix protein M1 is present underneath the lipid envelope and encases viral ribonucleoprotein (vRNP) complexes. The influenza virus buds from the apical plasma membrane (PM), which is divided by tight junctions in polarized epithelial cells (1). It is considered that all viral components are targeted to the apical PM, where particle budding occurs. HA, NA, and M2 are synthesized at the endoplasmic reticulum (ER) and are transported to the apical PM through the trans-Golgi network (TGN). The apical sorting signals were identified in the transmembrane domains (TMDs) of both HA and NA (2, 3). Many studies indicate that during the apical trafficking, HA and NA are associated with lipid raft microdomains, which are enriched in cholesterol and sphingolipids (3, 4), whereas M2 is excluded from these domains (5, 6). Several studies also indicate that the TMD and the cytoplasmic tail (CT) of HA and NA are important for their association with lipid rafts (3, 5, 7). It has been shown that, in the case of HA, palmitoylation at three conserved cysteines in the TMD-CT region is required for association with lipid rafts (8). A very recent study suggested that M2 was a key player in influenza virus particle budding, which is independent of the endosomal protein sorting complex required for transport (ESCRT) (9).

Lipid rafts are thought to function as platforms for selective concentration of raft-associated proteins to promote protein-protein interactions for their functions (10). Lipid rafts have also been shown to play pivotal roles in apical trafficking in polarized cells (11) and in signal transduction pathways, such as Ras signaling (12) and phosphatidylinositol 4,5-bisphosphate (PIP2) signaling (13). It has been suggested that for influenza virus HA and NA, the association with lipid rafts constitutes a part of the machinery necessary for apical trafficking in polarized cells (14, 15). Previous studies have indicated that disruption of lipid rafts by treatment with methyl-β-cyclodextrin (MβCD) and lovastatin delays the TGN-to-apical PM trafficking of HA and missorts HA to the ba-

Received 1 March 2014 **Accepted** 18 June 2014
Published ahead of print 25 June 2014
Editor: B. Williams
Address correspondence to Yuko Morikawa, morikawa@lisci.kitasato-u.ac.jp.

doi:10.1128/JVI.00586-14

solateral membrane, whereas vesicular stomatitis virus G protein, a nonraft-associated basolateral marker, remained unaffected (16), suggesting that raft association is required for apical transport of proteins. However, a number of studies have indicated that some mutations in the HA TMD and CT did not impair apical targeting of HA, irrespective of whether they caused significant reductions in the raft association (5, 7), suggesting that raft association is not essential for apical transport of HA.

Glycosylphosphatidylinositol (GPI)-anchored proteins (GPI-APs) are not integral membrane proteins but are associated with lipid rafts through the GPI moieties. In this group of proteins, the raft association is not a determinant for apical sorting because both apical and basolateral GPI-APs are associated with lipid rafts (17). Interestingly, only apical, but not basolateral, GPI-APs form oligomer complexes when they are associated with lipid rafts. When oligomerization of GPI-APs was impaired by mutations, the GPI-APs were missorted to the basolateral PM domain (17). A recent model has suggested that the oligomerization of GPI-APs promotes their stabilization in lipid rafts, leading to their incorporation into apical transport vesicles (10).

Influenza virus budding and release require the assembly of viral components, which occurs either during their trafficking to the apical PM or at the stage of particle budding (6, 18, 19). During the trafficking, all viral components, HA, NA, M2, M1, and vRNP, either individually or in their complex forms, are targeted to the apical PM and form a higher order of complex (7, 19, 20). Although the apical sorting determinants for individual viral components have been relatively well studied (2, 3), the molecular mechanisms and kinetics involved in their apical targeting have not been elucidated.

In this study, we focused on the kinetics of apical targeting of influenza virus envelope proteins in polarized MDCK cells. We found that HA and NA or M1, but not M2, mutually accelerated their apical PM targeting. Using TMD-CT mutants of HA and NA, we show that the association of HA and NA with lipid rafts is necessary for the acceleration of their apical PM targeting. Our data indicate that HA and NA come into close proximity (clustering) in lipid rafts upon coexpression. Our data also show the clustering of lipid rafts upon coexpression of HA and NA, suggesting a possible mechanism of accelerated apical transport of HA and NA via the clustering of lipid rafts.

MATERIALS AND METHODS

Viruses and plasmids. The H141Y and E142Q mutations were introduced into the HA gene of the influenza A/Puerto Rico/8/34 (PR8) virus by inverted PCR. This PR8 derivative is referred to as the wild-type (wt) strain in the present study. The authentic PR8 strain was used as the parental virus. The wt and mutant PR8 viruses were generated by a reverse genetics system with PolI plasmids (pHH21) and protein expression plasmids, as described previously (21). Briefly, 293T cells were transfected with PolI plasmids for synthesis of each viral RNA segment and protein expression plasmids for the PB1, PB2, PA, nucleoprotein (NP), HA, and NA. At 6 h posttransfection (hpt), the cell medium was replaced with Opti-MEM I (Gibco) supplemented with 5 μg/ml acetyl trypsin and 0.3% bovine serum albumin (BSA), and the cells were incubated for 2 or 3 days. Recovered viruses were grown in Madin-Darby canine kidney (MDCK) cells stably expressing HA (MDCK-HA) (the kind gift of N. Takizawa from the Institute of Microbial Chemistry, Japan).

The HA and NA constructs with deletion of the CT (ΔCT-HA and ΔCT-NA) for recovery of recombinant viruses have essentially been described elsewhere (22, 23). For ΔCT-HA, three consecutive stop codons were placed at the end of the TMD coding sequence, and the downstream nucleotide sequence was left intact. For ΔCT-NA, the authentic start codon was mutated, and a new start codon was created at the beginning of the TMD coding sequence. The constructs were cloned into pHH21. The HA and NA constructs with alanine substitutions in the CT (residues 557 to 559 of HA [HA557–559], HA560–563, HA564–566, residues 2 to 3 of NA [NA2–3], NA4–6, and NA2–6) and TMD (HA533–535, HA550–552, NA7–10, and NA31–35) and those with cysteine-to-serine substitutions at three palmitoylation sites (HA-SSS) were generated by overlapping PCR and were cloned into pHH21. The viruses with similar alanine substitutions have been described previously (3, 5, 8).

The open reading frames of the wt-HA, NA, M1, and M2 genes were cloned into the eukaryotic expression plasmid pCAGGS. The open reading frames of the HA and NA constructs with deletion of the CT and those with the alanine substitutions were similarly cloned into pCAGGS. The cDNAs encoding CD59, the 75-kDa neurotrophin receptor (p75), and their green fluorescent protein (GFP)-tagged versions (GFP-CD59 and p75-GFP) were also cloned into pCAGGS.

Cell culture, infection, and DNA transfection. MDCK and 293T cells were maintained in Dulbecco's modified Eagle's medium (Sigma) supplemented with 10% fetal bovine serum. MDCK cells were seeded into 12-well plates (1×10^6 cells/well) and were polarized by a 12-h incubation. The polarized MDCK cells were used throughout this study. The MDCK cells were infected with the wt virus at a multiplicity of infection (MOI) of 0.1 or 1 for 1 h. Transfection of DNA was carried out using Lipofectamine LTX (Invitrogen). To synchronize protein expression from plasmids, DNA-Lipofectamine complexes were sedimented by plate centrifugation at $250 \times g$ for 5 min. In some experiments, MDCK cells were transfected with DNA and subsequently superinfected with the authentic PR8 virus.

Virus growth and plaque assay. MDCK cells were inoculated with virus at an MOI of 0.1 in Opti-MEM I supplemented with 0.3% BSA for 1 h at 37°C. After being washed, the cells were incubated in Opti-MEM I supplemented with 5 μg/ml acetyl trypsin and 0.3% BSA. The culture medium was harvested at various time points and was subjected to plaque assay on MDCK or MDCK-HA cells.

Cholesterol depletion. For the inhibition of cholesterol synthesis, 293T and MDCK cells were pretreated with 8 μM lovastatin (Merck) for 12 h. After transfection, the cells were incubated in the presence of 8 μM lovastatin for 12 or 24 h. The cells were further treated with 5 or 10 mM methyl-β-cyclodextrin (MβCD) (Sigma) in the presence of 8 μM lovastatin for 1 h.

Indirect immunofluorescence assay. Polarized MDCK cells were grown on coverslips in 12-well plates and were either infected with virus or transfected with protein expression plasmids. The cells were fixed with 4% paraformaldehyde (PFA) and permeabilized with 0.5% Triton X-100 (TX-100). Following blocking, the cells were incubated with primary antibodies (Abs) and subsequently with secondary Abs conjugated with Alexa Fluor 488, 568, or 647 (Molecular Probes). The following Abs were used as primary Abs: mouse anti-HA mAb12-1G6 (24), mouse anti-HA Ab (TaKaRa), rabbit anti-NA Ab (Sino Biological), sheep anti-NA Ab (R&D Systems), rabbit anti-M1 polyclonal Ab (25), mouse anti-M2 Ab (Santa Cruz), mouse anti-NP mAb61A5 (26), mouse anti-CD59 Ab (Abcam), rabbit anti-TGN46 Ab (Abcam), rabbit anti-ZO-3 Ab (Invitrogen), and rabbit anti-caveolin-1 Ab (Santa Cruz). For costaining with HA and M2 or vRNP, anti-HA mAb12-1G6 was prelabeled by using a Zenon Alexa Fluor 488 mouse IgG1 labeling kit (Invitrogen), and the mouse anti-HA (TaKaRa), anti-M2, and anti-NP Abs were similarly prelabeled with Alexa Fluor 568, as described previously (24). Nuclear staining was carried out with TO-PRO-3 (Molecular Probes) or 4′,6′-diamidino-2-phenylindole (DAPI; Molecular Probes). The cells were observed with a laser scanning confocal microscope (TCS-SP5II AOBS; Leica). Confocal images were collected at 0.5-μm intervals along the *z* axis. Reconstitution of an *x-z* plane was processed using ImageJ software (27). Fifty antigen-positive cells were observed in each experiment, and patterns of antigen distribution were analyzed.

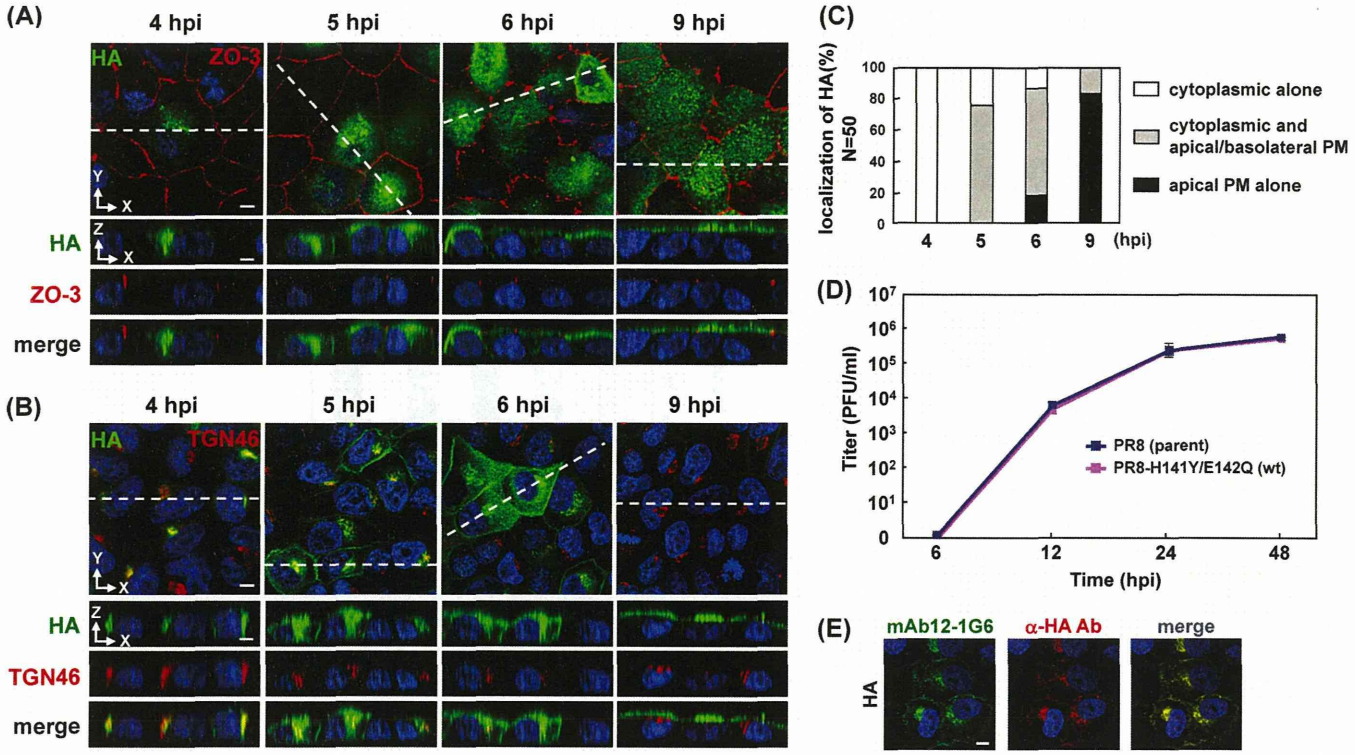

FIG 1 Temporal study of apical PM targeting of HA in infected cells and growth kinetics of virus. Polarized MDCK cells were infected with a PR8 derivative containing H141Y and E142Q substitutions in HA (referred to as wt in this study). At various time points (indicated), cells were stained with anti-HA mAb12-1G6, anti-ZO-3, and anti-TGN46 Abs. Localization of HA (green) and ZO-3 (red) (A) or TGN46 (red) (B) are shown in the *x-y* and *x-z* planes. Nuclei were stained with TO-PRO-3 (blue). The dashed lines in *x-y* images indicate the positions of *x-z* images. (C) For semiquantification of the HA localization in infected cells, 50 HA-positive cells were observed at each time point, and the number of cells with each distribution pattern of HA was counted. (D) MDCK cells were infected with the authentic PR8 (parent) or the PR8–H141Y/E142Q (wt) virus at an MOI of 0.1. At the indicated time points, an aliquot of the culture medium was harvested, and virus titers were measured by plaque assay on MDCK cells. (E) Polarized MDCK cells were infected with the wt virus. At 5 hpi, the cells were fixed and costained with prelabeled anti-HA mAb12-1G6 (green) and mouse anti-HA Ab (TaKaRa) (red). Nuclei were stained with TO-PRO-3 (blue). All images were taken at the same magnification. Scale bar, 10 μm. α, anti.

For quantitative analysis of HA and NA expression, polarized MDCK cells on coverslips in 12-well plates (1×10^6 cells/well) were singly transfected with an HA expression plasmid or cotransfected with the HA and an NA expression plasmids. After fixation with 4% PFA, the cells were incubated with mouse anti-HA Ab (TaKaRa) (for HA on the apical PM). The cells were refixed with 4% PFA and were permeabilized with 0.5% TX-100. The cells were incubated with rabbit anti-NA Ab (Sino Biological) (for total NA) and subsequently with anti-mouse IgG conjugated with Alexa Fluor 647 and anti-rabbit IgG conjugated with Alexa Fluor 568. For total HA, the cells were refixed with 4% PFA and blocked with nonspecific mouse Ig. The cells were finally incubated with anti-HA mAb12-1G6 prelabeled by using a Zenon Alexa Fluor 488 mouse IgG labeling kit (Invitrogen). Nuclear staining was carried out with DAPI (Molecular Probes). Confocal images were collected at 0.5-μm intervals along the *z* axis. In each cell, the sum of intensity values of a *z* stack was calculated as a *z*-projection image by the "sum slices" command of ImageJ. In each acquired channel, single cell area and mean fluorescence intensities (MFIs; arbitrary units) were measured. The MFIs of the Alexa Fluor 488 and 568 channels were evaluated as total expression levels of HA and NA in each cell, respectively. The total fluorescence intensity (MFI × area) of HA divided by that of NA was evaluated as the expression ratio of HA to NA. The cells (39 to 45 cells) were subjected to analysis of HA distribution patterns (either apical PM alone or PMs plus cytoplasmic compartments). Sparse MDCK cells (1×10^5 cells/well) were also used in the experiment shown in Fig. 3C.

TX-100 solubilization analysis and coimmunoprecipitation. 293T cells were seeded into 12-well plates (5×10^5 cells/well) or 10-cm-diameter dishes (5×10^6 cells/dish). The cells were singly transfected with HA and NA expression plasmids or cotransfected with a combination of HA and NA, HA and M1, or HA and GFP-CD59 expression plasmids. At 24 hpt, the cells were resuspended with cold TNE buffer (50 mM Tris-HCl [pH 7.5], 1 mM EDTA, and 150 mM NaCl) containing 1 mM dithiothreitol (DTT) and protease inhibitor Complete Mini cocktail (Roche). After brief sonication, the samples were treated with 1% TX-100 at 4°C or 37°C for 30 min and then centrifuged at 17,400 × *g* for 30 min at 4°C to separate the soluble and insoluble fractions. For TX-100 solubilization analysis, both the supernatants and pellets were adjusted to be the same volume with TNE buffer and analyzed by Western blotting. For coimmunoprecipitation, the supernatants were mixed with 10 μg of anti-HA mAb12-1G6 and were incubated at 4°C for 90 min. The supernatants were subsequently mixed with preblocked protein G-Sepharose beads (GE Healthcare) and were incubated at 4°C for 60 min. After samples were washed with TNE buffer containing 0.1% TX-100 three times, immunoprecipitates were eluted from the beads by boiling with SDS sample buffer and analyzed by Western blotting with sheep anti-NA Ab (R&D Systems) and rabbit anti-M1 polyclonal Ab (25). GFP-CD59 was detected with mouse anti-GFP Ab (Sigma).

***In situ* PLA.** An *in situ* proximity ligation assay (PLA) was performed according to the manufacturer's instructions (Olink Biosciences). Briefly, polarized MDCK cells were either transfected with combinations of protein expression plasmids or were infected with virus. At 9 hpt or 3.5 or 5 h postinfection (hpi), the cells were fixed with 4% PFA and permeabilized with 0.5% TX-100. After a blocking step, the cells were incubated with mouse anti-HA mAb12-1G6, rabbit anti-NA Ab, mouse anti-GFP Ab, or

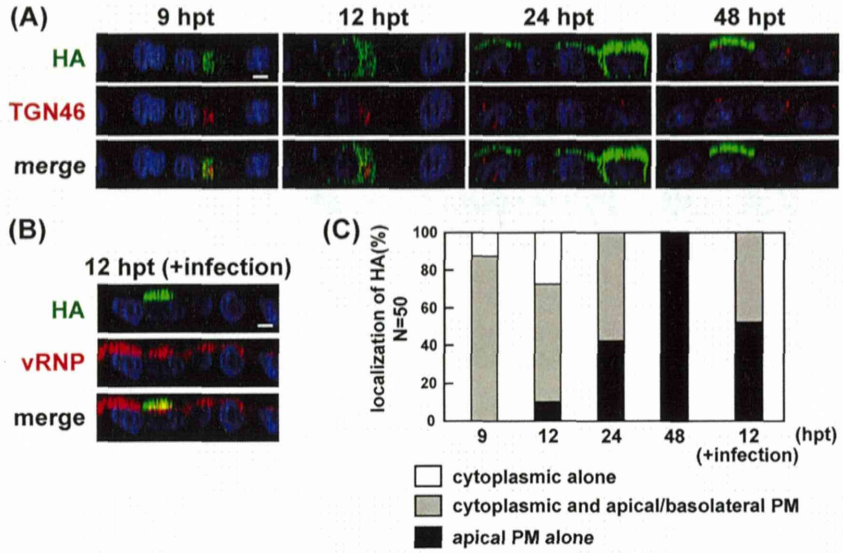

FIG 2 Temporal study of apical PM targeting of HA in transfected cells and acceleration of the apical targeting upon superinfection. (A) Polarized MDCK cells were transfected with a plasmid expressing wt HA. At various time points (indicated), the cells were stained with anti-HA mAb12-1G6 and anti-TGN46 Ab. Localizations of HA (green) and TGN46 (red) are shown in the *x-z* plane. (B) Polarized MDCK cells were similarly transfected with a plasmid expressing wt-HA. At 6 hpt, the cells were infected with the authentic PR8 strain (parent) of influenza virus. At 12 hpt, the cells were stained with prelabeled mAb12-1G6 (green; only reactive with wt-HA) and anti-NP Ab (red; for detection of superinfection). Nuclei were stained with TO-PRO-3 (blue). Localizations of HA (green) and vRNP (red) are shown in the *x-z* plane. All images were taken at the same magnification. Scale bar, 10 μm. (C) For semiquantification of the HA localization, 50 mAb12-1G6-reactive (transfected) HA-positive cells were observed at each time point, and the number of cells with each distribution pattern of HA was counted.

rabbit caveolin-1 Ab (Santa Cruz) for 1 h at room temperature. After being washed, the cells were incubated with two species-specific secondary antibodies conjugated with unique oligonucleotides (anti-rabbit Plus and anti-mouse Minus) as PLA probes. Phosphorylated connector oligonucleotides were hybridized to the PLA probes. If the PLA probes are present in close proximity (<40 nm), the phosphorylated oligonucleotides are formed in a circular template by a ligase. This template was subsequently amplified by rolling-circle amplification with DNA polymerase and was detected with fluorescently labeled complementary oligonucleotide probes (Duolink Detection Kit Red). TGN46 was stained with rabbit anti-TGN46 Ab prelabeled by using a Zenon Alexa Fluor 488 rabbit IgG labeling kit (Invitrogen). The PLA signals were observed by confocal microscopy, and the number of signals was automatically counted with BlobFinder software (28). Data are shown as means with standard deviations from two independent experiments (at least 10 cells). Statistical significance was determined by Student's *t* test. *P* values of <0.05 were considered statistically significant.

Treatment with Endo H. Polarized MDCK cells (1×10^6 cells/well) were transfected with HA and/or NA expression plasmids. At 12 hpt, the cells were resuspended with cold phosphate-buffered saline and sonicated. The protein samples were denatured and subsequently digested with endoglycosidase H (Endo H; New England BioLabs) for 1 h at 37°C. The samples were analyzed by Western blotting with rabbit anti-HA Ab (Sino Biological) and sheep anti-NA Ab (R&D Systems). As control, 20 μM brefeldin A was added to the cells at 6 hpt.

RESULTS

Apical PM targeting of HA in singly transfected cells was slower than that of HA in infected cells. HA is transported to the apical PM via the secretory pathway in polarized cells (1). We have previously generated an anti-HA monoclonal antibody (mAb12-1G6) that specifically binds to the loop (amino acid sequence QGKS at positions 142 to 145) of the head domain in H5 HA (24). We found that mAb12-1G6 failed to detect the authentic PR8 HA but did detect HA when it contained H141Y and E142Q substitutions without any reduction in infectivity (Fig. 1D). When prelabeled mAb12-1G6 and commercial mouse anti-HA Ab (TaKaRa) were used for costaining, their staining patterns were identical (Fig. 1E), suggesting that mAb12-1G6 did not detect a specific HA population. Thus, we used the PR8 derivative containing H141Y and E142Q mutations as the wild-type (wt) strain in the present study and investigated apical PM targeting of HA.

To understand the overall kinetics of intracellular trafficking of HA, we initially carried out a time course study. Polarized MDCK cells were infected with the wt PR8 virus and were subjected to immunofluorescent assays at various time points (4, 5, 6, and 9 hpi) with mAb12-1G6 and anti-ZO-3 (for tight junctions) or anti-TGN46 (for TGN) Ab (Fig. 1A and B). Anti-ZO-3 Ab was used to differentiate the apical from the basolateral PM. The TGN is the major sorting organelle in the cytoplasmic trafficking pathways (29). Serial confocal *z* sections were collected at 0.5-μm intervals from the top to the bottom of cells. As shown in the *x-z* plane (Fig. 1A and B), three patterns of HA distribution (cytoplasmic compartments; cytoplasmic compartments and both apical and basolateral PMs; only at the apical PM) were observed. We observed 50 HA-positive cells at each time point and sorted them into the three categories (Fig. 1C). At 4 hpi, all HA antigens were observed in the cytoplasmic compartments (100% of HA-positive cells), most likely at the TGN. At 5 hpi, HA was observed both in the cytoplasmic compartments and at the apical/basolateral PMs (76% of HA-positive cells). At 6 hpi, the majority of HA was still localized to the cytoplasmic compartments and at the apical/basolateral PMs (70% of HA-positive cells), but a population of HA had accumulated at the apical PM in some cells (17% of HA-positive cells). HA accumulation at the apical PM became evident at 9 hpi (83% of HA-positive cells) (Fig. 1B and C). HA has been suggested to be transported initially to the basolateral PM and then to the apical